Reduction Potentials of Rieske Clusters: Importance of the Coupling between Oxidation State and Histidine Protonation State†

Yanbing Zu,‡ Manon M.-J. Couture,§ Derrick R. J. Kolling,|| Antony R. Crofts,|| Lindsay D. Eltis,⊥ James A. Fee,# and Judy Hirst*,‡

Medical Research Council Dunn Human Nutrition Unit, Wellcome Trust/MRC Building, Hills Road, Cambridge, CB2 2XY, United Kingdom, Department of Biochemistry, Université Laval, Québec, Canada, G1K 7P4, Department of Biochemistry and Center for Biophysics and Computational Biology, University of Illinois at Urbana-Champaign, Champaign, Illinois 61801, Departments of Microbiology and Immunology and Biochemistry and Molecular Biology, University of British Columbia, Canada, V6T 1Z3, and Division of Biology, University of California at San Diego, La Jolla, California 92093 and Department of Molecular Biology, The Scripps Research Institute, 10550 North Torrey Pines Road, La Jolla, California 92037

Received June 25, 2003; Revised Manuscript Received September 2, 2003

ABSTRACT: Rieske [2Fe−2S] clusters can be classified into two groups, depending on their reduction potentials. Typical high-potential Rieske proteins have pH-dependent reduction potentials between +350 and +150 mV at pH 7, and low-potential Rieske proteins have pH-independent potentials of around −150 mV at pH 7. The pH dependence of the former group is attributed to coupled deprotonation of the two histidine ligands. Protein-film voltammetry has been used to compare three Rieske proteins: the high-potential Rieske proteins from *Rhodobacter sphaeroides* (*Rs*Rp) and *Thermus thermophilus* (*Tt*Rp) and the low-potential Rieske ferredoxin from *Burkholderia* sp. strain LB400 (BphF). *Rs*Rp and *Tt*Rp differ because there is a cluster to serine hydrogen bond in *Rs*Rp, which raises its potential by 140 mV. BphF lacks five hydrogen bonds to the cluster and an adjacent disulfide bond. Voltammetry measurements between pH 3 and 14 reveal that all the proteins, including BphF, have pH-dependent reduction potentials with remarkably similar overall profiles. Relative to *Rs*Rp and *Tt*Rp, the potential versus pH curve of BphF is shifted to lower potential and higher pH, and the pK_a values of the histidine ligands of the oxidized and reduced cluster are closer together. Therefore, in addition to simple electrostatic effects on *E* and pK_a, the reduction potentials of Rieske clusters are determined by the degree of coupling between cluster oxidation state and histidine protonation state. Implications for the mechanism of quinol oxidation at the Q_O site of the cytochrome bc_1 and b_6f complexes are discussed.

Rieske iron−sulfur [2Fe−2S] clusters play important roles in the respiratory and photosynthetic quinol/cytochrome *c* oxidoreductases (the cytochrome bc_1 and b_6f complexes) and in bacterial oxygenases, such as those involved in the catabolism of aromatic compounds (*1*). The Rieske clusters from the cytochrome bc_1 and b_6f complexes are distinguished by their high and pH-dependent reduction potentials (*2*−*5*), whereas the Rieske clusters from dioxygenase-associated ferredoxins have lower, pH-independent, potentials (*6*, *7*). At pH 7, Rieske cluster potentials span over 600 mV. The highest reported value, +490 mV at low pH, is from the cytochrome bc_1 complex of the acidophilic proteobacterium, *Thiobacillus ferrooxidans* (*8*). More typically, Rieske cluster potentials range from +350 mV for a ubiquinol or plastoquinol oxidizing cytochrome bc_1 or b_6f complex to −150 mV for a Rieske-type ferredoxin (*1*).

In Rieske clusters, two histidine ligands coordinate the redox-active iron center (*9*−*11*). At low pH, these ligands are formally uncharged. However, it is generally accepted that in the high-potential proteins they deprotonate as the pH is increased, rendering the reduction potential pH-dependent (*4*, *12*−*14*). For the high-potential Rieske cluster from *Thermus thermophilus*, *Tt*Rp,[1] the decrease in reduction potential that occurs when both histidines deprotonate is approximately 440 mV (*15*). In contrast, [2Fe−2S] clusters that are ligated by four cysteine ligands have pH-independent reduction potentials: their ligands are always negatively charged, and the clusters have the same charge as a fully deprotonated Rieske cluster.

The high reduction potentials of respiratory-type Rieske centers are essential for energy transduction since they must

† This work was supported by The Medical Research Council, by NSERC Operating Grant 171359 (L.D.E.), and by NIH Grants GM35438 (A.R.C.) and GM35342 (J.A.F.).

* To whom correspondence should be addressed. Tel: +44 1223 252810. Fax: +44 1223 252815. E-mail: jh@mrc-dunn.cam.ac.uk.

‡ Medical Research Council Dunn Human Nutrition Unit.

§ Université Laval.

|| University of Illinois at Urbana-Champaign.

⊥ University of British Columbia.

University of California at San Diego and The Scripps Research Institute.

[1] Abbreviations: BphF, Rieske ferredoxin from *Burkholderia* sp. strain LB400; *E*, potential; PFV, protein film voltammetry; PGE, pyrolytic graphite edge; *Tt*Rp, soluble Rieske domain (residues 38−210) from the cytochrome bc_1 complex of *Thermus thermophilus*; *Rs*Rp, Rieske protein from the cytochrome bc_1 complex of *Rhodobacter sphaeroides*; SHE, standard hydrogen electrode.

10.1021/bi0350957 CCC: $25.00
Published on Web 10/07/2003

be high enough to initiate the catalytic oxidation of bound quinol at the Q_O site (*16*). Point mutations, which decrease the reduction potential, also decrease the catalytic activity, suggesting that quinol oxidation by the Rieske cluster may be the rate-determining step in catalysis (*17*−*19*). Furthermore, the Rieske proteins from quinol/cytochrome *c* oxidoreductases that oxidize menaquinol, rather than ubiquinol or plastoquinol, have reduction potentials that are decreased by approximately 150 mV, in line with the different quinone potentials (*20*).[2] This illustrates that it is essential to tune the cluster reduction potential to optimize its physiological role. It has also been proposed that deprotonation of one of the histidine ligands is essential to the oxidoreductase function: that the Rieske cluster extracts a proton, as well as an electron, from bound quinol (*16*, *19*, *22*, *23*). Therefore, the histidine pK_a values may also be mechanistically important. In the oxidized state, the lowest histidine pK_a value is typically 7.5, four to five units lower than in the reduced state (*14*, *15*). Consequently, at physiological pH, the reduction of a deprotonated Rieske cluster is strongly coupled, thermodynamically, to its reprotonation.

How the high potentials, and the low histidine pK_a values, of Rieske clusters in quinol/cytochrome *c* oxidoreductases are determined is not fully understood. The overall structure of the cluster binding subdomain is highly conserved between both high- and low-potential Rieske proteins, and the clusters are exposed to solvent to a similar degree (*11*, *24*−*27*). A disulfide bridge is adjacent to the cluster in only the high-potential proteins but is unlikely to exert a significant effect on reduction or deprotonation (*28*). Several conserved hydrogen bonds, from amino acid side chains and main-chain amides, interact with the high-potential clusters and contribute to their increased reduction potentials (*11*, *17*, *18*, *26*, *27*). However, it is not clear how much they affect the histidine pK_a values. Moreover, the lack of pH-dependence in the low-potential proteins, throughout the physiological region, appears inconsistent with the solvent exposure of their histidine residues. Although a comprehensive understanding of coupled electron−proton transfer is crucial for the elucidation of energy transduction mechanisms, how electron transfer is coupled to proton transfer at Rieske clusters has not been addressed directly. Iron−sulfur clusters are also implicated in coupled proton-transfer reactions in respiratory complex I (NADH/quinone oxidoreductase) (*29*), nickel−iron (*30*) and iron-only (*31*) hydrogenases, and nitrogenase (*32*), and many enzymes contain active sites at which proton-coupled redox reactions occur. In contrast, low-potential Rieske-type ferredoxins are simple electron-transfer proteins, not adapted for coupled proton transfer.

Protein-film voltammetry (PFV) was used previously to characterize the respiratory-type *Tt*Rp (*15*). Reversible voltammetric signals spanning a wide potential range were observed between pH 3 and 14, allowing the thermodynamics of cluster reduction and histidine deprotonation to be described comprehensively. The potential is pH-independent at low pH, where both histidines are protonated, and at high pH, where both histidines are deprotonated. The histidines deprotonate at pH 7.85 and 9.65 in the oxidized cluster and at approximately pH 12.5 in the reduced cluster. Therefore, between pH 7.85 and 9.65, one proton is released when the cluster is oxidized, but between pH 9.65 and 12.5, two protons are released. The thermodynamic coupling between reduction and protonation is significant: the reduction potential decreases by almost 450 mV from its acid limit to its alkaline limit.

Herein, we describe the use of PFV to compare the redox behavior of three different Rieske proteins, *Rs*Rp, *Tt*Rp, and BphF. *Rs*Rp, the Rieske cluster from the cytochrome bc_1 complex of *Rhodobacter sphaeroides* is a high-potential, pH-dependent Rieske protein from a ubiquinol oxidizing enzyme. *Tt*Rp is from a menaquinol oxidizing cytochrome bc_1 complex and therefore has a lower, pH-dependent reduction potential. BphF, a low-potential Rieske protein, is the soluble ferredoxin associated with the biphenyl dioxygenase of *Burkholderia* sp. strain LB400. Each Rieske cluster potential is reported over a wide range of pH values and is used to define the electron and proton affinities. In conjunction with known structural information, a detailed picture is constructed of how the reduction potentials and pK_a values of Rieske clusters are determined.

EXPERIMENTAL PROCEDURES

*Protein Preparation. Rs*Rp was isolated intact from the cytochrome bc_1 complex; the hydrophobic N-terminal domain was retained. The cytochrome bc_1 complex was prepared as described previously (*33*). For fractionation, it was exchanged into a solution containing 10 mM CAPS and 0.01% DM (*n*-decyl-*β*-D-maltoside) at pH 12, incubated on ice for 30 min, and filtered using a Centriplus centrifugal concentrator with a cutoff of 50 kDa. The Rieske protein was contained in the filtrate. It was exchanged into 20 mM histidine, pH 7.5, 0.5 mM EDTA, 1% glycerol (v/v), and 500 mM KCl and concentrated with a 7 kDa cutoff concentrator. The soluble domain (residues 38−210) of the Rieske protein from *T. thermophilus* (*Tt*Rp), and BphF, were heterologously expressed and purified as described previously (*7*, *26*).

Protein-Film Voltammetry. Reduction potentials were measured using PFV as described previously (*28*, *34*). Briefly, the protein was applied directly to a freshly polished pyrolytic graphite edge electrode surface and then placed into solution in an all-glass cell. The cell was thermostated and encased in a Faraday cage and an anaerobic glovebox (O_2 ∼1 ppm, Belle Technology, Portesham, UK). Analogue-scan cyclic voltammetry was performed using an Autolab electrochemical analyzer (Eco-chemie, Utrecht, The Netherlands). Data were analyzed using Fourier transformation and an in-house analysis program (courtesy of Dr. H. A. Heering). Solution pH values were controlled using mixtures of four of the following buffers (total concentration, 40 mM): 10 mM sodium acetate, HEPES, MES, TAPS, CAPS, and sodium phosphate, depending on the pH. Volumetric solutions of NaOH were used above pH 13. All standard reagents were supplied by Fluka or Merck-BDH. The pH of each solution was checked immediately following measurement; 1 M NaOH was used as a pH 14 standard. The effects of high Na^+ concentration were corrected using standard formulas (*35*).

[2] The reduction potentials of plastoquinone, ubiquinone, and menaquinone are estimated to be +110, +70, and −60 mV at pH 7, respectively (*20*, *21*).

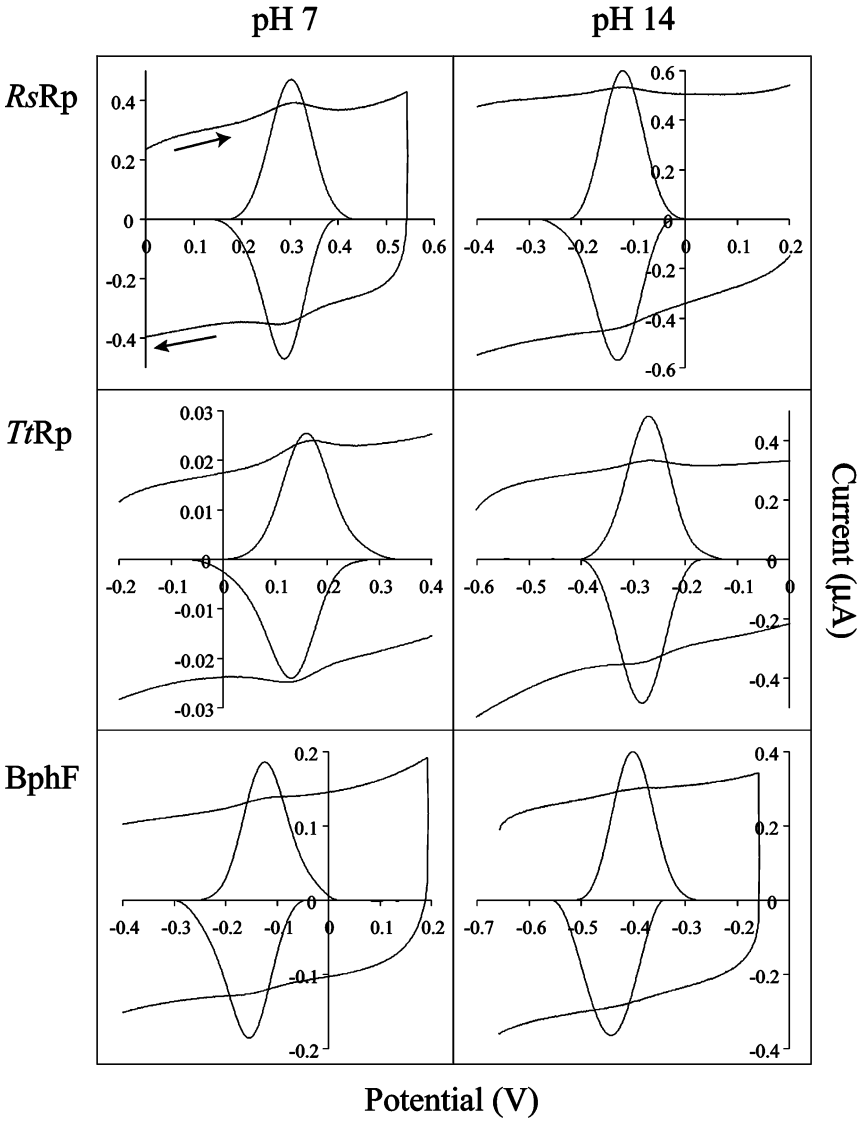

FIGURE 1: Voltammograms recorded for each Rieske protein, adsorbed on the electrode surface, in solutions of pH 7 and 14 (*Rs*Rp: 7.05, 14.0; *Tt*Rp: 7.09, 14.0; BphF: 6.95, 14.0). The raw data are displayed alongside background subtracted signals, which have been corrected for the effects of electrode capacitance and surface reactions, and which are adjusted in magnitude such that a theoretically shaped (Nernstian) peak would have an amplitude equal to the *y*-axis span. Therefore, peak areas on each graph are equivalent. The *x*-axis covers 0.6 V in each case, although the range is shifted to allow for the different peak potentials. All voltammograms were recorded at 20 mV s^{-1}, 20 °C, solution conditions as described in the Experimental Procedures using 2 M NaCl.

RESULTS

Reversible Protein-Film Voltammetry (PFV) Measurements. All three Rieske proteins, *Rs*Rp, *Tt*Rp, and BphF, could be adsorbed directly to a freshly polished pyrolytic graphite edge (PGE) electrode. Upon cycling of the electrode potential, clearly defined oxidation and reduction peaks were observed; these signals were not present in the absence of adsorbed protein. Typical examples for each protein, at pH 7 and 14, are shown in Figure 1, where raw data are displayed alongside the normalized peaks obtained by correction for the electrode background. Peak half-height widths and separations were close to their ideal Nernstian values and did not decrease if the scan rate was decreased. Therefore, the voltammetry is reversible, the interfacial electron transfer is facile, and the layer of adsorbed protein is thermodynamically homogeneous.[3] Protein surface coverages were maximally 2.5×10^{-11}, 2.2×10^{-11}, and 1.4×10^{-11} mol cm^{-2} for *Rs*Rp, *Tt*Rp, and BphF, respectively, consistent with the formation of a monolayer or submonolayer of protein. The reduction potential is the average potential of the forward and reverse peaks of Figure 1. In each case, the reduction potentials are ionic-strength dependent, particularly at low pH, as described previously for *Tt*Rp (*15*). The ionic-strength dependence is believed to be due to changes in the protein charge with pH (*34*, *36*), an effect that can be dampened-out by high ionic strength. Therefore, all the data reported here were obtained in 2 M NaCl, to display only the intrinsic pH-dependent properties of the Rieske clusters.

Potentials Measured by PFV Correspond Closely to Those Measured in Solution. The close correspondence of potentials

[3] Interfacial electron transfer to the BphF cluster is less rapid than to the *Rs*Rp and *Tt*Rp clusters since (i) peak separations are 40 mV at 20 mV s^{-1} (as compared to 15 and 25 mV for *Rs*Rp and *Tt*Rp, respectively) and (ii) at scan rates above 10 V s^{-1}, no clear redox signals could be observed. For *Tt*Rp and *Rs*Rp, signals remained obvious at scan rates above 1000 V s^{-1}.

measured by PFV with those measured in solution confirms that adsorption-induced structural changes were negligible. CD-monitored redox titrations for the Rieske protein in the isolated cytochrome bc_1 complex and membranes of *R. sphaeroides* gave a reduction potential of 300 mV at pH 7.0 and E_{acid}, pK_{ox1}, and pK_{ox2} values (see below) of 315 mV, 7.6, and 9.8, respectively (*22*). PFV studies of *Rs*Rp gave 280 mV at pH 7.0 (0.1 M NaCl) and E_{acid}, pK_{ox1}, and pK_{ox2} values of 308 mV, 7.6, and 9.6 in 2 M NaCl. Small differences may be due to variation in the experimental conditions. In addition, the potential of the cluster in the cytochrome bc_1 complex depends on the conformation of the Rieske protein within the complex because of alterations to the hydrogen bonding network around the cluster (*37*). For *Tt*Rp, voltammetric experiments were performed over a range of conditions (pH 4−8, 0.01, 0.1, and 2 M NaCl, 0 °C) with the protein diffusing; potentials differed from their PFV equivalents by less than 25 mV. The potential measured spectroelectrochemically, ~140 mV (pH 7, 75 mM Tris-HCl) (*3*), is close to the PFV measurement of 132 mV (pH 7, 0.1 M NaCl).

For BphF, reduction potentials were measured previously by diffusional voltammetry in solutions containing 2 mM neomycin (*7*). At pH 7.0 (22 °C), the value reported is −157 mV, for comparison with the PFV measurement of −160 mV in an identical solution. However, adsorption promoters such as neomycin were avoided throughout the work described here since they had a significant effect on the measured potentials. In an identical buffer lacking neomycin, BphF yielded a potential of −180 mV by PFV. The effect of neomycin was greater in low ionic-strength solutions: in 0.01 M NaCl, the reduction potential increased from −196 to −153 mV upon the addition of 2 mM neomycin, but in 2 M buffer it did not change (therefore, neomycin has a significant effect on the ionic-strength dependence). Similar effects have been described previously and may be due to coadsorbate−protein interactions or to the coadsorbate producing a surface-constrained region of a high dielectric that mimics high ionic-strength conditions (*34*).

Reduction Potential Measurements at High pH. Figure 1 shows that reversible voltammetric signals can be observed up to pH 14. To confirm that changes in the reduction potential observed at such an alkaline pH were reversible, protein films were switched repeatedly between solutions of high and low pH (*15*). The potentials of *Rs*Rp and *Tt*Rp responded to pH exactly as expected. For BphF, the signal intensity decreased significantly when the protein film was exposed to high pH. However, weak signals at the potential expected were observed upon returning to low pH. Similarly, the redox signals of *Rs*Rp and *Tt*Rp were stable for at least 10 cycles above pH 12, while the signals from BphF were observable for only one or two cycles. In previous diffusional voltammetry studies of BphF, signals observed above pH 10 were too weak to interpret (*7*). These data suggest that the Rieske cluster in BphF is less stable, perhaps due to the lack of an adjacent disulfide bond and several hydrogen bonds (*11*, *27*).

All Three Rieske Clusters Have pH-Dependent Reduction Potentials. Figure 2 shows how the reduction potential of each Rieske center varies between pH 3 and 14. The three curves display the same overall shape, but they are shifted significantly with respect to one another. The two high-potential proteins are pH-dependent above pH 7. In contrast, the potential of BphF is pH-independent up to pH 10. This is the first time that the full pH-dependence of a low-potential Rieske cluster has been reported because previous studies only accessed lower pH values (*1*, *6*, *7*). As described previously for *Tt*Rp (*15*), the pH-dependent reduction potentials can be modeled using the thermodynamic cycle presented in Scheme 1 and eq 1 derived from it (*38*)

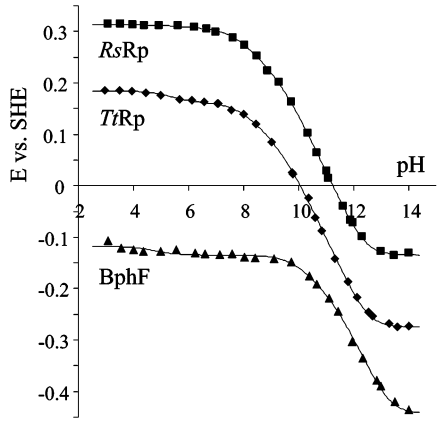

FIGURE 2: Variation of reduction potential with pH for each Rieske protein: *Rs*Rp (■), *Tt*Rp (◆), and BphF(▲) in 2 M NaCl (solution conditions as described in the Experimental Procedures). Fits to the data, obtained using eq 1 and Scheme 1, are shown, and the corresponding E and pK_a values are reported in Table 1.

Scheme 1: Thermodynamic Square Scheme Describing Coupled Proton and Electron Transfer to Rieske Clusters[a]

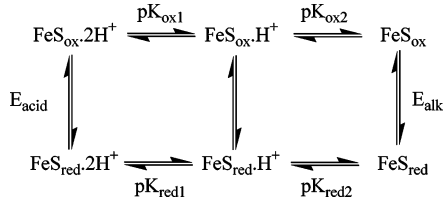

[a] E_{acid} and E_{alk} are the pH-independent reduction potentials at the acid and alkaline limits, respectively. pK_{ox1} and pK_{ox2} are the pK_a values for the two histidine ligands when the cluster is oxidized; pK_{red1} and pK_{red2} are the corresponding values for the reduced cluster.

$$E_{obs} = E_{alk} - \frac{RT}{F}\ln\left[\left(1 + \frac{a_{H^+}}{K_{ox2}} + \frac{a_{H^+}^2}{K_{ox1}K_{ox2}}\right)\Big/ \left(1 + \frac{a_{H^+}}{K_{red2}} + \frac{a_{H^+}^2}{K_{red1}K_{red2}}\right)\right] \quad (1)$$

In Scheme 1 and eq 1, pK_{ox1}, pK_{ox2}, pK_{red1}, and pK_{red2} refer to the pK_a values of the oxidized and reduced cluster; they are assigned to the two cluster-ligating histidine residues (*4*, *12*−*14*). E_{alk} is the reduction potential of the cluster at the alkaline limit, when both histidines are fully deprotonated. Correspondingly, E_{acid} will denote the reduction potential at the acid limit. The fitted curves obtained using eq 1 are shown along with the experimental data in Figure 2; values for the six constants are reported in Table 1. Figure 3 shows a Pourbaix diagram for each cluster, to illustrate the pH values and potentials at which the different protonation and redox states are the most thermodynamically favored. Four distinct regions of pH are observed for each cluster: (i) at low pH, below both pK_{ox1} and pK_{ox2}, the reduction potential is pH-independent, and the histidines remain fully protonated

Table 1: Reduction Potentials and pK_a Values for the Three Rieske Proteins[a]

	pK_{ox1}	pK_{ox2}	pK_{red1}	pK_{red2}	ΔpK	E_{acid}	E_{alk}	ΔE
*Rs*Rp	7.6 ± 0.1	9.6 ± 0.1	12.4 ± 0.4	12.4 ± 0.4	3.8	308 ± 3	−134 ± 6	442
*Tt*Rp	7.85 ± 0.15	9.65 ± 0.12	12.5 ± 0.5	12.5 ± 0.5	3.75	161 ± 4	−275 ± 8	436
BphF	9.8 ± 0.2	11.5 ± 0.4	13.3 ± 0.8	13.3 ± 0.8	2.65	−135 ± 5	−441 ± 20	306
	ΔpK_{ox1}	ΔpK_{ox2}	ΔpK_{red1}	ΔpK_{red2}		ΔE_{acid}	ΔE_{alk}	
*Rs*Rp vs *Tt*Rp	0.15	0.05	0.10	0.10		−147	−141	
*Rs*Rp vs BphF	2.20	1.90	0.90	0.90		−443	−307	

[a] The parameters are defined in Scheme 1. ΔpK is the difference between the average of pK_{ox1} and pK_{ox2} and the average of pK_{red1} and pK_{red2}. Error values are estimated 95% confidence intervals. The larger errors in pK_{red1} and pK_{red2} allow for their possible separation.

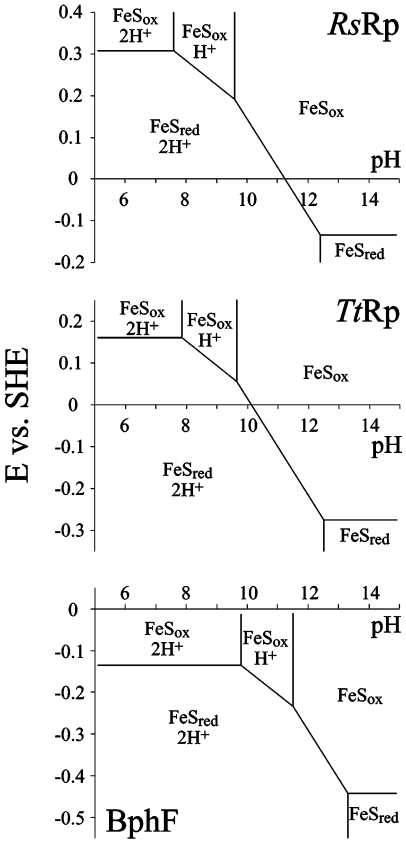

FIGURE 3: Pourbaix diagrams for each of the three Rieske proteins, *Rs*Rp, *Tt*Rp, and BphF. The diagrams show which redox state and which protonation state are the most thermodynamically favored, over a range of potentials and pH values. The parameters used are derived from the data fits shown in Figure 2.

in each oxidation state. (ii) At pK_{ox1} < pH < pK_{ox2}, one histidine is deprotonated, but only in the oxidized state: the gradient of the curve is theoretically −58 mV per decade. (iii) At pK_{ox2} < pH < p$K_{red1,2}$, both histidines are deprotonated in the oxidized state but protonated in the reduced state: the gradient of the curve is theoretically −116 mV per decade. (iv) Above pK_{red1} and pK_{red2}, the reduction potential is again pH-independent, as both histidines are deprotonated in both oxidation states. Because there is no clear region, at high pH, in which the gradient tends toward −58 mV per decade before it reaches the alkaline limit and becomes pH-independent, our data have been modeled using equal values of pK_{red1} and pK_{red2}. This produces a good fit to the data for all three proteins but does not rule out the possibility that pK_{red1} and pK_{red2} are separated by a small amount, particularly in BphF, for which fewer data points were obtained at high pH. The differences between pK_{ox1} and pK_{red1}, pK_{ox2} and pK_{red2}, and E_{acid} and E_{alk} are proportional to the amounts by which the electron and proton sense one another: to the degree of interaction (or coupling) between electron- and proton-transfer events at the cluster.

Enthalpy and Entropy of Reduction. The temperature dependence of the reduction potential was measured for each Rieske protein at pH 7 and 14. These two pH values represent E_{alk} and E_{acid} and were chosen since there is no contribution from coupled protonation events. Potentials were measured from 5 to 35 °C in a nonisothermal cell, and the pH of each solution was checked immediately after voltammetry, at the experimental temperature. Several measurements were recorded around pH 7 and then interpolated to provide an exact value. The variation of reduction potential with temperature is linear, and ΔS^0_{obs} could therefore be calculated from the first derivative ($= nF(dE/dT)$). Since the reference electrode was held at constant temperature, it does not contribute to ΔS^0_{obs}; therefore, $\Delta S^0_{FeS} = \Delta S^0_{obs}$ (*39*). Values for ΔS^0_{FeS} are presented in Table 2. At each temperature, $\Delta G^0_{tot} = -nFE$, and since all values were corrected to the standard hydrogen electrode scale, ΔG^0_{tot} refers to the following reaction:

$$FeS_{ox} + {}^1/_2H_2 \Leftrightarrow FeS_{red} + H^+ \qquad (2)$$

Values for ΔG^0_{tot} are presented in Table 2 at 25 °C. To calculate ΔH^0_{tot}, the standard enthalpy change for the SHE half-reaction (65 J K^{-1} mol^{-1}) was added to ΔS^0_{FeS} to give the value for ΔS^0_{tot} that relates to eq 2 (*39*). Values for ΔS^0_{tot} and ΔH^0_{tot} are presented in Table 2. Our values at pH 7 are consistent with values reported previously for the bovine protein (*4*, *6*), the low-potential ferredoxin from the benzene dioxygenase of *Pseudomonas putida* ML2 (*6*), and BphF (*7*).

DISCUSSION

(i) Single Scheme for Coupled Electron−Proton Transfer at Rieske Clusters. A single reaction scheme, Scheme 1, describes coupled electron−proton-transfer events at all Rieske clusters (see Figure 2). Two pK_a values, ascribed to deprotonation of the two histidine ligands, are always required for each redox state.

For the reduced cluster, the apparent pK_a values of the histidine ligands are high (see Table 1), and they differ by less than 2 units from the pK_a value of free imidazole (14.2) (*40*). However, there is no clear region of pH in which only one proton is bound to the reduced cluster: in each case, the pH-dependence appears to switch from −116 mV per decade at pK_{ox2} < pH < p$K_{red1,2}$ (two protons are bound upon reduction) to pH-independent at pH > p$K_{red1,2}$ (the protein remains fully deprotonated upon reduction). Because of difficulties in defining accurately the pH values of alkaline solutions containing high concentrations of Na^+, and because

Table 2: Free Energy, Enthalpy, and Entropy of Reduction of Each of the Three Rieske Proteins at pH 7 and 14

	ΔG^0_{tot} (25 °C) kJ mol^{-1}	ΔH^0_{tot} kJ mol^{-1}	$-T\Delta S^0_{tot}$ (25 °C) kJ mol^{-1}	ΔS^0_{tot} J K^{-1} mol^{-1}	ΔS^0_{FeS} J K^{-1} mol^{-1}
			pH 7		
*Rs*Rp	−29.7 ± 0.2	−68.4 ± 2.4	38.7 ± 2.4	−130 ± 8	−65 ± 8
*Tt*Rp	−15.5 ± 0.2	−51.6 ± 2.4	36.1 ± 2.4	−121 ± 8	−56 ± 8
BphF	13.0 ± 0.2	−5.2 ± 1.5	18.5 ± 1.5	−62 ± 5	3 ± 5
*Rs*Rp − BphF	−42.7 ± 0.3	−63.2 ± 2.8	20.2 ± 2.8	−68 ± 9	−68 ± 9
			pH 14		
*Rs*Rp	12.9 ± 0.2	−21.1 ± 3.9	34.0 ± 3.9	−114 ± 13	−49 ± 13
*Tt*Rp	26.5 ± 0.2	−3.3 ± 0.8	29.8 ± 0.8	−100 ± 2	−35 ± 2
BphF	42.6 ± 0.2	23.0 ± 1.8	20.0 ± 1.8	−67 ± 6	−2 ± 6
*Rs*Rp − BphF	−29.7 ± 0.3	−44.1 ± 4.3	14.0 ± 4.3	−47 ± 14	−47 ± 14
			pH 7−14		
*Rs*Rp	−42.6 ± 0.3	−47.3 ± 4.6	4.7 ± 4.6	16 ± 15	16 ± 15
*Tt*Rp	−42.0 ± 0.3	−48.3 ± 2.5	6.3 ± 2.5	21 ± 5	21 ± 5
BphF	−29.6 ± 0.3	−28.2 ± 2.3	1.5 ± 2.3	−5 ± 8	−5 ± 8

predicted variations in the shape of the curve are subtle, it is not possible currently to determine unique values for pK_{red1} and pK_{red2}. Therefore, for simplicity, our data have been modeled using pK_{red1} = pK_{red2}; they exclude the possibility that pK_{red1} is significantly less than pK_{red2} but do not exclude the possibility that pK_{red1} is higher than pK_{red2} (implying that the two protons bind cooperatively in the reduced state). The characteristics of the fully deprotonated Rieske cluster are currently under further investigation.

For the oxidized form of each protein, three protonation states are apparent: fully protonated (pH < pK_{ox1}), singly protonated (pK_{ox1} < pH < pK_{ox2}), and fully deprotonated (pH > pK_{ox2}); the protons are removed sequentially as the pH is increased. The pK_a values deviate further from the value for free imidazole than with the cluster reduced (see Table 1), most simply because Fe^{III} exerts a greater electrostatic effect than Fe^{II} (*15*).

This is the first time that the pH-dependent reduction potential of a low-potential Rieske protein has been described. Our success has relied upon the speed of our measurements: PFV experiments are complete within 30 s of the initial immersion of the film; therefore, they do not rely upon long-term stability of the protein in the experimental solution (*41*). It is clear that the reduction potentials of the low-potential proteins were classified previously as pH-independent because of the limited pH range available (*1*, *6*, *7*) and that, as expected from atomic resolution structural models which show that the histidine ligands of both the high- and the low-potential proteins are solvent exposed (*27*), their histidine ligands also deprotonate at high pH.

(ii) Comparison of the Two High-Potential Rieske Proteins. The reduction potential versus pH curve for *Rs*Rp is very similar to that of *Tt*Rp, but it is shifted (along the ordinate) to a higher potential. E_{acid} and E_{alk} are shifted by the same amount (see Table 1), indicating that the difference is due to an extra positive charge or dipole, close to the reducible iron center, in *Rs*Rp. However, the pK_a values for both proteins are very close (there is little shift along the abscissa, see Table 1, and the difference in reduction potential is pH-independent). Therefore, the extra positive charge or dipole does not affect the deprotonation of the histidine nitrogen centers significantly, consistent with them being spatially separated from the redox center and exposed to solvent.

The structure of the soluble fragment of the Rieske protein isolated from the bovine cytochrome bc_1 complex (PDB 1RIE, (*11*)) is our model for *Rs*Rp. In the bovine protein, Ser163 (Ser158 in *Rs*Rp) provides a hydrogen bond to the cluster (Ser-Oγ to S1). In *Tt*Rp, the hydrogen-bonding network to the cluster is largely conserved except that a glycine replaces this serine (PDB 1NYK (*26*)). It is likely that this hydrogen bond accounts for the difference between *Rs*Rp and *Tt*Rp: the $O^{\delta-}-H^{\delta+}$ dipole pulls electron density from the cluster core, preferentially stabilizing the reduced, electron-rich state (*42*), and the strength of the hydrogen bond increases upon cluster reduction. The serine appears to be conserved in Rieske proteins from enzymes that oxidize ubiquinone (such as *Rs*Rp) or plastoquinone but not in their lower-potential menaquinone-oxidizing counterparts, such as *Tt*Rp (*20*, *26*). Mutating the serine residue to alanine in *Paracoccus denitrificans* and *Saccharomyces cerevisae* caused decreases in potential of 95 mV (pH 6.0) and 130 mV (pH 7.0) (*17*, *18*). In *Rs*Rp and *Tt*Rp, the corresponding effect on the histidine pK_a values is negligible (<10 mV); this aspect is discussed below.

(iii) Comparison of the High- and Low-Potential Rieske Proteins. The high- and low-potential proteins differ due to changes in both the electrostatic potential and the coupling between reduction and protonation. Comparison of the pH-dependent reduction potentials of *Rs*Rp and BphF (Figure 2) shows that, unlike *Rs*Rp and *Tt*Rp, they are not related simply by translation along the potential and pH axes but that for *Rs*Rp, the differences between E_{acid} and E_{alk}, and between p$K_{red1,2}$ and p$K_{ox1,2}$, are significantly larger than for BphF (see Table 1). Therefore, in *Rs*Rp, the redox center responds more strongly to the protonation state and vice versa: the coupling is stronger.

Hydrogen Bonding to the Cluster: the Effect of Electrostatics. Comparison of the structures of BphF (PDB 1FQT), the bovine Rieske protein (*11*), and the Rieske protein from spinach chloroplasts (*24*) indicated that the lower potential of BphF results from the relative absence of five hydrogen bonds to the cluster (*27*). In *Rs*Rp and *Tt*Rp, these hydrogen bonds preferentially stabilize the reduced cluster and increase its reduction potential. They are from Ser158-Oγ to S1 (*Rs*Rp only, see previously), Tyr160-Oη to Cys133-Sγ, and from the amide bonds of His156 (cluster ligand) to S1, Leu136 to S2, and Cys138 (disulfide bond) to S2. The hydrogen

bonds from both the serine (see previously) and the tyrosine increase the reduction potential significantly. Tyrosine mutations in *S. cerevisae* (*17*), *P. denitrificans* (*18*), and *R. sphaeroides* (*19*) decreased the cluster potential by typically 60 mV. Therefore, together, the serine and tyrosine residues account for around 170 mV. Interactions from the three backbone amides are expected to be weaker than those from the $O^{\delta-}-H^{\delta+}$ dipoles. They may be structurally supported by the disulfide bond in *Rs*Rp and *Tt*Rp (*27*), although it is unlikely that the disulfide has a significant direct effect (*28*). Therefore, the difference in the E_{acid} values of *Rs*Rp and BphF, 443 mV (Table 1), is unlikely to be completely accounted for by five extra hydrogen bonds to the cluster in *Rs*Rp.

The hydrogen bonds may also decrease the proton affinities of the two histidines: indeed, the p*K* values of *Rs*Rp are significantly lower than those of BphF (Figures 2 and 3 and Table 1). Considering $pK_{red1,2}$ (because the reduced state is less affected by the charge on the iron), the hydrogen bonds reduce the p*K* values by only 0.9 units. Therefore, the total shift for the two histidines is 1.8 units, thermodynamically equivalent to 24% of the shift in potential. The decreased effect is due to two factors: (i) in contrast to the iron center, the histidine rings are exposed to solvent, screening them from buried partial charges and (ii) the hydrogen bonds are farther removed from the N−H imidazole bond, both in terms of bonds (four more) and in terms of through-space distance. (In the bovine Rieske protein (*11*) and *Tt*Rp (*26*), the average dipole to histidine distance is 7.7 Å but only 5.3 Å to the iron.) The effects on the pK_a values of the serine and tyrosine mutations in *P. denitrificans* and *S. cerevisae* were not reported (*17*, *18*); in *R. sphaeroides*, the Y156F mutation did not alter pK_{ox1} significantly (*19*). Therefore, the significant difference in the pK_a values of the high- and low-potential proteins cannot be explained satisfactorily by the hydrogen-bonding dipoles.

The effects of the hydrogen bonds are also reflected in the enthalpies of reduction (Table 2). ΔH^0_{tot} values for *Rs*Rp and *Tt*Rp are considerably more negative than for BphF, at both pH 7 and 14, and differences in ΔH^0_{tot} dominate the differences in ΔG^0_{tot}. Although negative enthalpies of reduction indicate increased bonding upon reduction, the extra electron on the iron-center is antibonding.[4] Therefore, the increased bonding is due to the strengthening of the hydrogen-bonding network around the cluster, upon reduction of the high-potential proteins, consistent with the $O/N^{\delta-}-H^{\delta+}$ dipoles orientated toward the cluster core. Furthermore, the increased rigidity decreases the conformational freedom; therefore, entropies of reduction for *Rs*Rp and *Tt*Rp are significantly more negative than for BphF (Table 2).

Coupling between Cluster Redox State and Histidine Protonation State. In both *Rs*Rp and BphF, the cluster oxidation state is coupled to the histidine protonation state. The reduction potential is lower when the histidines are deprotonated because the neutral imidazoles are electron withdrawing and favor reduction, whereas the negatively charged imidazolates favor oxidation. Correspondingly, the pK_a is lower when the cluster is oxidized, as the more positively charged Fe^{III} favors deprotonation. However, in *Rs*Rp, the redox and protonation states are more strongly interdependent than in BphF. The coupling strength is proportional to the differences between E_{acid} and E_{alk} and between the average of $pK_{ox1,2}$ and $pK_{red1,2}$ (ΔpK, see Table 1). For *Rs*Rp and BphF, ΔpK is 3.8 and 2.65 units, respectively, and $E_{acid} - E_{alk}$ is 442 and 306 mV, respectively. Similarly, the increased reduction potential of the protonated cluster has been identified with an increase in the N−H bond strength upon reduction (*15*). The enthalpy changes at pH 7 and 14 differ much more for *Rs*Rp and *Tt*Rp than for BphF (see Table 2), again demonstrating that the coupling between reduction and protonation is smaller in BphF.

Inspection of the structures of the bovine Rieske protein (*11*), *Tt*Rp (*26*), and BphF (*27*) reveals that the decreased coupling in BphF may be due to increased access of solvent dipoles to the active site. In each case, the cluster and iron-center geometries are very similar. Iron−histidine bond lengths are unchanged, although small variations in the N−Fe−N bond angle and in the tilt of the plane of the imidazole ring of the second histidine ligand (in the sequence) with respect to the cluster rhomboid are apparent. These may reflect minor variations in N(His)−Fe bonding, particularly in π back-bonding from the iron to the imidazole (*43*), but they are insufficient to explain the different coupling strengths. However, reduction and deprotonation may be coupled electrostatically, as well as electronically. Although the distances between the redox center and the protonation sites are conserved, electrostatic coupling depends on the intervening medium as well as the distance. In the high-potential proteins, 23% of the first ligand (in the sequence) is solvent accessible,[5] and 45% of the second is solvent-accessible. For BphF, the corresponding values are 38 and 45%, and so the exposure of the first histidine is significantly higher. The redox-active iron centers of the bovine Rieske protein (≈*Rs*Rp) and *Tt*Rp are 5.9 and 5.8 Å from the nearest structurally resolved water molecules, respectively, but that of BphF is only 4.3 Å away. Access of water molecules into the intervening protein structure, as a result of thermal fluctuations or because of structural changes upon histidine deprotonation, may also be greater in BphF. Therefore, the cluster in BphF is more solvent exposed, and the coupling between cluster redox state and histidine protonation state is screened out. A key determinant of the solvent accessibility of the active site is the hydrophobic side chain of a leucine residue, replaced by glycine in BphF. In agreement with our proposal, the L136G mutation in the *R. capsulatus* cytochrome bc_1 complex decreased the Rieske cluster potential by 114 mV (from 310 to 196 mV at pH 7) (*45*).

Finally, for cysteine-ligated iron−sulfur clusters, the negative charge on the cluster increases upon reduction (−2 to −3), increasing the solvent ordering. Therefore, more solvent accessible clusters have more negative entropies of reduction (*46*). In contrast, the more solvent accessible BphF cluster has a less negative entropy of reduction than *Tt*Rp or *Rs*Rp. However, there is little difference between the entropies of reduction at pH 14 (the charges on the Rieske cluster are the same as for a cysteine-ligated [2Fe−2S] cluster) and at pH 7 (the charge on the cluster changes from 0 to −1). This suggests strongly that solvent effects are not

[4] This may be the origin of the positive enthalpy change observed for BphF at pH 14.

[5] Solvent accessible surface areas were determined using a 1.4 Å probe, by using GETAREA (http://www.scsb.utmb.edu/ (*44*)).

Scheme 2: Thermodynamic Square Scheme Describing Coupled Proton and Electron Transfer between the Rieske Cluster and Bound Quinol[a]

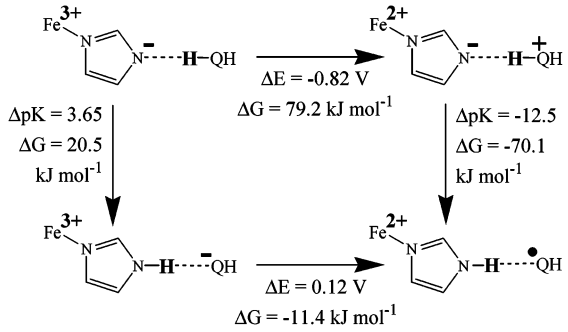

[a] The reaction begins with the top, left-hand species upon binding of the deprotonated Rieske protein and finishes with the bottom, right-hand species and the dissociation of the protonated and reduced Rieske protein. The thermodynamic parameters for the Rieske protein are taken from Scheme 1 and Table 1, and those for ubiquinol/one are the consensus values cited by Rich (*21*).

predominant in determining the entropies of reduction of Rieske proteins, and that, as described previously, they are determined mostly by contraction of the hydrogen-bonding network around the cluster.

(iv) Biological Implications and Summary. In respiratory cytochrome bc_1 and photosynthetic b_6f complexes, the rate of catalytic quinol oxidation decreases markedly as the reduction potential of the Rieske center is decreased (*17*−*19*), suggesting that electron transfer from quinol to the Rieske cluster is rate limiting. However, since a constant difference is maintained between the cluster and the quinone potentials, (*20*) unnecessarily high cluster potentials appear to have a detrimental effect, perhaps on stability or on cluster reoxidation by cytochrome c_1. Clearly, the Rieske cluster potential is tuned for optimal overall performance. The high reduction potential at physiological pH is strongly dependent upon (i) the histidine ligands being protonated so that they have high electronegativity and neutral charge and (ii) upon the coupling between cluster reduction and histidine protonation: pK_{ox1} and pK_{ox2} must be significantly lower than $pK_{red1,2}$ to elevate the reduction potential as the pH is decreased. Coupling is both by the cluster electronic structure and by electrostatic interaction; electrostatic coupling is increased by the exclusion of solvent from the active site. The reduction potential is increased further by hydrogen bonding, to delocalize the increased electron density on the reduced cluster (*1*). Rieske-type ferredoxins have lower potentials at physiological pH because there are fewer hydrogen bonds to the cluster (*27*) and because increased solvent accessibility weakens the coupling between reduction and protonation.

The mechanistic details of the redox reaction between the Rieske center and the bound quinol, in the cytochrome bc_1 and b_6f complexes, are still debated. It has been suggested that quinol binding involves a hydrogen bond from the quinol −OH to the Nϵ of one of the histidine ligands (*23*, *47*), and in the stigmatellin-inhibited enzyme, there is no hydrogen-bonding network linking the quinol/histidine hydrogen bond to bulk solvent (*48*). These suggest the possibility of coupling proton transfer to electron transfer from quinol to the Rieske cluster and using the histidine ligand to shuttle the proton out of the Q_O site (*22*, *23*, *49*). The following properties of high-potential Rieske proteins, as discussed previously, are consistent with this proposal. (i) pK_{ox1} values are low (see Table 1); thus, the singly deprotonated form is thermodynamically accessible: since deprotonation is fast (*15*), it represents a preequilibrium process. (ii) The reduced Rieske proteins have very high pK_a values (see Table 1); therefore, proton uptake upon reduction is imperative. (iii) The strong coupling between electron transfer and proton transfer (ΔE and ΔpK are large) optimizes the efficiency and is promoted by the exclusion of solvent from the active site.

Finally, although our results do not suggest directly a mechanism for the putative coupled electron−proton-transfer event, they do define the thermodynamic cycle (Scheme 2), using experimentally determined values. The free energies required to access the two possible intermediates (Scheme 2, top right and bottom left) are 79.2 kJ and 20.5 kJ mol^{-1}; thus, on this basis, the preferred route is proton transfer followed by electron transfer (*50*). Overall, the free-energy is regained on the second step. However, since both possible intermediates are highly unstable, a concerted electron−proton-transfer reaction along the diagonal, involving a single transition state for the simultaneous transfer of both species, appears energetically more likely (*51*).

REFERENCES

1. Link, T. A. (1999) The structures of Rieske and Rieske-type proteins, *Adv. Inorg. Chem. 47*, 83−157.
2. Prince, R. C., and Dutton, P. L. (1976) Further studies on the Rieske iron−sulfur center in mitochondrial and photosynthetic systems: a pK_a on the oxidized form, *FEBS Lett. 65*, 117−119.
3. Kuila, D., and Fee, J. A. (1986) Evidence for a redox-linked ionizable group associated with the [2Fe−2S] cluster of *Thermus* Rieske protein, *J. Biol. Chem. 261*, 2768−2771.
4. Link, T. A., Hagen, W. R., Pierik, A. J., Assmann, C., and von Jagow, G. (1992) Determination of the redox properties of the Rieske [2Fe−2S] cluster of bovine heart bc_1 complex by direct electrochemistry of a water-soluble fragment, *Eur. J. Biochem. 208*, 685−691.
5. Nitschke, W., Joliot, P., Liebl, U., Rutherford, A. W., Hauska, G., Müller, A., and Riedel, A. (1992) The pH dependence of the redox midpoint potential of the 2Fe2S cluster from cytochrome b_6f complex (the Rieske center), *Biochim. Biophys. Acta 1102*, 266−268.
6. Link, T. A., Hatzfeld, O. M., Unalkat, P., Shergill, J. K., Cammack, R., and Mason, J. R. (1996) Comparison of the Rieske [2Fe−2S] center in the bc_1 complex and in bacterial dioxygenases by circular dichroism spectroscopy and cyclic voltammetry, *Biochemistry 35*, 7546−7552.
7. Couture, M. M.-J., Colbert, C. L., Babini, E., Rosell, F. I., Mauk, A. G., Bolin, J. T., and Eltis, L. D. (2001) Characterization of BphF, a Rieske-type ferredoxin with a low reduction potential, *Biochemistry 40*, 84−92.
8. Brugna, M., Nitschke, W., Asso, M., Guigliarelli, B., Lemesle-Meunier, D., and Schmidt, C. (1999) Redox components of cytochrome *bc*-type enzymes in acidophilic prokaryotes, *J. Biol. Chem. 274*, 16766−16772.
9. Cline, J. F., Hoffman, B. M., Mims, W. B., LaHaie, E., Ballou, D. P., and Fee, J. A. (1985) Evidence for N coordination to Fe in the [2Fe−2S] clusters of *Thermus* Rieske protein and phthalate dioxygenase from *Pseudomonas*, *J. Biol. Chem. 260*, 3251−3254.
10. Gurbiel, R. J., Batie, C. J., Sivaraja, M., True, A. E., Fee, J. A., Hoffman, B. M., and Ballou, D. P. (1989) Electron−nuclear double resonance spectroscopy of ^{15}N-enriched phthalate dioxygenase from *Pseudomonas cepacia* proves that two histidines are coordinated to the [2Fe−2S] Rieske-type clusters, *Biochemistry 28*, 4861−4871.
11. Iwata, S., Saynovits, M., Link, T. A., and Michel, H. (1996) Structure of a water soluble fragment of the Rieske iron−sulfur protein of the bovine heart mitochondrial cytochrome bc_1 complex determined by MAD phasing at 1.5 Å resolution, *Structure 4*, 567−579.

12. Link, T. A. (1994) Two p*K* values of the oxidized Rieske [2Fe−2S] cluster observed by CD spectroscopy, *Biochim. Biophys. Acta 1185*, 81−84.
13. Kuila, D., Schoonover, J. R., Dyer, R. B., Batie, C. J., Ballou, D. P., Fee, J. A., and Woodruff, W. H. (1992) Resonance Raman studies of Rieske-type proteins, *Biochim. Biophys. Acta 1140*, 175−183.
14. Ullmann, G. M., Noodleman, L., and Case, D. A. (2002) Density functional calculation of pK_a values and redox potentials in the bovine Rieske iron−sulfur protein, *J. Biol. Inorg. Chem. 7*, 632−639.
15. Zu, Y., Fee, J. A., and Hirst, J. (2001) Complete thermodynamic characterization of reduction and protonation of the bc_1-type Rieske [2Fe−2S] center of *Thermus thermophilus*, *J. Am. Chem. Soc. 123*, 9906−9907.
16. Berry, E. A., Guergova-Kuras, M., Huang, L.-S., and Crofts, A. R. (2000) Structure and function of cytochrome *bc* complexes, *Annu. Rev. Biochem. 69*, 1005−1075.
17. Denke, E., Merbitz-Zahradnik, T., Hatzfeld, O. M., Snyder, C. H., Link, T. A., and Trumpower, B. L. (1998) Alteration of the midpoint potential and catalytic activity of the Rieske iron−sulfur protein by changes of amino acids forming hydrogen bonds to the iron−sulfur cluster, *J. Biol. Chem. 273*, 9085−9093.
18. Schröter, T., Hatzfeld, O. M., Gemeinhardt, S., Korn, M., Friedrich, T., Ludwig, B., and Link, T. A. (1998) Mutational analysis of residues forming hydrogen bonds in the Rieske [2Fe−2S] cluster of the cytochrome bc_1 complex in *Paracoccus denitrificans*, *Eur. J. Biochem. 255*, 100−106.
19. Guergova-Kuras, M., Kuras, R., Ugulava, N., Hadad, I., and Crofts, A. (2000) Specific mutagenesis of the Rieske iron−sulfur protein in *Rhodobacter sphaeroides* shows that both the thermodynamic gradient and the p*K* of the oxidized form determine the rate of quinol oxidation by the bc_1 complex, *Biochemistry 39*, 7436−7444.
20. Liebl, U., Pezennec, S., Riedel, A., Kellner, E., and Nitschke, W. (1992) The Rieske FeS center from the Gram-positive bacterium PS3 and its interaction with the menaquinone pool studied by EPR, *J. Biol. Chem. 267*, 14068−14072.
21. Rich, P. R. (1984) Electron and proton transfers through quinones and cytochrome *bc* complexes, *Biochim. Biophys. Acta 768*, 53−79.
22. Ugulava, N., and Crofts, A. R. (1998) CD-monitored redox titration of the Rieske Fe−S protein of *Rhodobacter sphaeroides*: pH dependence of the midpoint potential in the isolated bc_1 complex and in membranes, *FEBS Lett. 440*, 409−413.
23. Crofts, A. R., Hong, S., Ugulava, N., Barquera, B., Gennis, R., Guergova-Kuras, M., and Berry, E. A. (1999) Pathways for proton release during ubihydroquinone oxidation by the bc_1 complex, *Proc. Natl. Acad. Sci. U.S.A. 96*, 10021−10026.
24. Carrell, C. J., Zhang, H., Cramer, W. A., and Smith, J. L. (1997) Biological identity and diversity in photosynthesis and respiration: structure of the lumen-side domain of the chloroplast Rieske protein, *Structure 5*, 1613−1625.
25. Bönisch, H., Schmidt, C. L., Schäfer, G., and Ladenstein, R. (2002) The structure of the soluble domain of an archaeal Rieske iron−sulfur protein at 1.1 Å resolution, *J. Mol. Biol. 319*, 791−805.
26. Hunsicker-Wang, L., Heine, A., Chen, Y., Luna, E. P., Todaro, T., Zhang, Y., Williams, P. A., McRee, D. E., Hirst, J., Stout, C. D., and Fee, J. A. (2003) High-resolution structure of the soluble, respiratory-type Rieske protein from *Thermus thermophilus*: Analysis and comparison, *Biochemistry 42*, 7303−7317.
27. Colbert, C. L., Couture, M. M.-J., Eltis, L. D., and Bolin, J. T. (2000) A cluster exposed: structure of the Rieske ferredoxin from biphenyl dioxygenase and the redox properties of Rieske Fe−S proteins, *Structure 8*, 1267−1278.
28. Zu, Y., Fee, J. A., and Hirst, J. (2002) Breaking and reforming the disulfide bond at the high-potential, respiratory-type [2Fe−2S] center of *Thermus thermophilus*: characterization of the sulfhydryl state by protein-film voltammetry, *Biochemistry 41*, 14054−14065.
29. Hirst, J. (2003) The dichotomy of complex I: a sodium ion pump or a proton pump, *Proc. Natl. Acad. Sci. U.S.A. 100*, 773−775.
30. Garcin, E., Montet, Y., Volbeda, A., Hatchikian, E. C., Frey, M., and Fontecilla-Camps, J. C. (1998) Structural bases for the catalytic mechanism of [NiFe] hydrogenases, *Biochem. Soc. Trans. 26*, 396−401.
31. Nicolet, Y., Lemon, B. J., Fontecilla-Camps, J. C., and Peters, J. W. (2000) A novel FeS cluster in Fe-only hydrogenases, *Trends Biochem. Sci. 25*, 138−143.
32. Einsle, O., Tezcan, F. A., Andrade, S. L. A., Schmid, B., Yoshida, M., Howard, J. B., and Rees, D. C. (2002) Nitrogenase MoFe protein at 1.16 Å resolution: a central ligand in the FeMo cofactor, *Science 297*, 1696−1700.
33. Guergova-Kuras, M., Salcedo-Hernandez, R., Bechmann, G., Kuras, R., Gennis, R. B., and Crofts, A. R. (1999) Expression and one-step purification of a fully active polyhistidine-tagged cytochrome bc_1 complex from *Rhodobacter sphaeroides*, *Protein Expr. Purif. 15*, 370−380.
34. Zu, Y., Di Bernardo, S., Yagi, T., and Hirst, J. (2002) Redox properties of the [2Fe−2S] center in the 24 kDa (NQO2) subunit of NADH:ubiquinone oxidoreductase (complex I), *Biochemistry 41*, 10056−10069.
35. Bard, A. J., and Faulkner, L. R. (2001) in *Electrochemical Methods*, 2nd ed., Wiley, New York.
36. Shifman, J. M., Moser, C. C., Kalsbeck, W. A., Bocian, D. F., and Dutton, P. L. (1998) Functionalized de novo designed proteins: mechanism of proton coupling to oxidation/reduction in heme protein maquettes, *Biochemistry 37*, 16815−16827.
37. Darrouzet, E., Valkova-Valchanova, M., and Daldal, F. (2002) The [2Fe−2S] cluster E_m as an indicator of the iron−sulfur subunit position in the ubihydroquinone oxidation site of the cytochrome bc_1 complex, *J. Biol. Chem. 277*, 3464−3470.
38. Clark, W. M. (1960) Oxidation−reduction potentials of organic systems, Ch. 4, Williams and Wilkins, Baltimore.
39. Taniguchi, V. T., Sailasuta-Scott, N., Anson, F. C., and Gray, H. B. (1980) Thermodynamics of metalloprotein electron-transfer reactions, *Pure Appl. Chem. 52*, 2275−2281.
40. Winter, J. A., Caruso, D., and Shepherd, R. E. (1988) Influence of pentaamminechromium(III) on the acidity of coordinated imidazoles and pyrazole, *Inorg. Chem. 27*, 1086−1089.
41. Armstrong, F. A., Heering, H. A., and Hirst, J. (1997) Reactions of complex metalloproteins studied by protein-film voltammetry, *Chem. Soc. Rev. 26*, 169−179.
42. Rose, K., Shadle, S. E., Glaser, T., de Vries, S., Cherepanov, A., Canters, G. W., Hedman, B., Hodgson, K. O., and Solomon, E. I. (1999) Investigation of the electronic structure of 2Fe−2S model complexes and the Rieske protein using ligand K-edge X-ray absorption spectroscopy, *J. Am. Chem. Soc. 121*, 2353−2363.
43. Johnson, C. R., Shepherd, R. E., Marr, B., O'Donnell, S., and Dressick, W. (1980) Affinities of imidazolate and imidazole ligands for pentacyanoiron(III), *J. Am. Chem. Soc. 102*, 6227−6235.
44. Fraczkiewicz, R., and Braun, W. (1998) Exact and efficient analytical calculation of the accessible surface areas and their gradients for macromolecules, *J. Comput. Chem. 19*, 319−333.
45. Liebl, U., Sled, V. D., Brasseur, G., Ohnishi, T., and Daldal, F. (1997) Conserved nonliganding residues of the *Rhodobacter capsulatus* Rieske iron−sulfur protein of the bc_1 complex are essential for protein structure, properties of the [2Fe−2S] cluster, and communication with the quinone pool, *Biochemistry 36*, 11675−11684.
46. Battistuzzi, G., D'Onofrio, M., Borsari, M., Sola, M., Macedo, A. L., Moura, J. J. G., and Rodrigues, P. (2000) Redox thermodynamics of low-potential iron−sulfur proteins, *J. Biol. Inorg. Chem. 5*, 748−760.
47. Zhang, Z., Huang, L., Shulmeister, V. M., Chi, Y.-I., Kim, K. K., Hung, L.-W., Crofts, A. R., Berry, E. A., and Kim, S.-H. (1998) Electron transfer by domain movement in cytochrome bc_1, *Nature 392*, 677−684.
48. Hunte, C., Koepke, J., Lange, C., Roβmanith, T., and Michel, H. (2000) Structure at 2.3 Å resolution of the cytochrome bc_1 complex from the yeast *Saccharomyces cerevisiae* cocrystallized with an antibody Fv fragment, *Structure 8*, 669−684.
49. Hunte, C., Palsdottir, H., and Trumpower, B. L. (2003) Proton-motive pathways and mechanisms in the cytochrome bc_1 complex, *FEBS Lett. 545*, 39−46.
50. Crofts, A. R., Guergova-Kuras, M., Kuras, R., Ugulava, N., Li, J., and Hong, S. (2000) Proton-coupled electron transfer at the Q_O-site: what type of mechanism can account for the high activation barrier? *Biochim. Biophys. Acta 1459*, 456−466.
51. Brunschwig, B. S., and Sutin, N. (1989) Directional electron-transfer−conformational interconversions and their effects on observed electron-transfer rate constants, *J. Am. Chem. Soc. 111*, 7454−7465.

BI0350957